FLUORESCENCE DETECTION OF GLUTATHIONE USING N-DOPED GRAPHENE QUANTUM DOTS−MnO_2 NANOARCHITECTURE **

Zhi-Mei Li [1], Ting Pi [1], Ya-Ping Sheng [2], Xiang-Juan Zheng [1,3*]

[1] College of Chemistry, Nanchang University, Nanchang 330031, China;
e-mail: zhengxiangjuan@ncu.edu.cn
[2] School of Chemistry and Materials Science, University of Science and Technology of China, Hefei 230026, China
[3] Jiangxi Key Laboratory for Multiscale Interdisciplinary Study, Nanchang, 330031, China

We build a novel fluorescence resonance energy transfer (FRET) method based on N-doped graphene quantum dots (NGQDs)-MnO_2 nanocomposite for rapid, sensitive detection of glutathione (GSH) levels in human serum. In this strategy, MnO_2 nanosheets on the NGQDs surface serve as a quencher. NGQDs fluorescence can make a recovery by the addition of GSH, which can reduce MnO_2 to Mn^{2+}, and thus the GSH can be monitored. The MnO_2 platform affords minimal background and high sensitivity for detecting GSH in this proposed scheme. Meanwhile, relevant fluorescence on-off-on processes were monitored, and the sensing mechanism was explored.

Keywords: *MnO_2, graphene quantum dots, fluorescence resonance energy transfer, glutathione.*

ФЛУОРЕСЦЕНТНОЕ ОБНАРУЖЕНИЕ ГЛУТАТИОНА С ИСПОЛЬЗОВАНИЕМ НАНОСИСТЕМЫ N-ЛЕГИРОВАННЫЕ ГРАФЕНОВЫЕ КВАНТОВЫЕ ТОЧКИ–MnO_2

Zh.-M. Li [1], T. Pi [1], Y.-P. Sheng [2], X.-J. Zheng [1,3*]

УДК 535.37;620.3

[1] Химический колледж Наньчанского университета, Наньчан 330031, Китай,
e-mail: zhengxiangjuan@ncu.edu.cn
[2] Школа химии и материаловедения Китайского университета науки и технологий, Хэфэй 230026, Китай
[3] Главная лаборатория многоуровневых междисциплинарных исследований Цзянси, Наньчан, 330031, Китай

(Поступила 23 августа 2019)

Предложен флуоресцентный метод определения уровней глутатиона (GSH) в сыворотке крови человека с использованием нанокомпозита квантовых точек графена (NGQD) и MnO_2, легированного N. Нанолисты MnO_2 на поверхности NGQD служат в качестве тушителя. Флуоресценция NGQD может восстанавливаться за счет добавления GSH, который восстанавливает MnO_2 до Mn_2^+, таким образом можно контролировать уровень GSH. Платформа MnO_2 обеспечивает минимальный фон и высокую чувствительность для обнаружения GSH в предлагаемой схеме. Отслежены соответствующие процессы включения-выключения флуоресценции и исследован механизм восприятия.

Ключевые слова: *MnO_2, графеновые квантовые точки, резонансный перенос энергии флуоресценции, глутатион.*

Introduction. In recent years, layered two-dimensional (2D) nanomaterial with single or few atomic layers have attracted growing attention owing to its unusual and fascinating physical and chemical properties such as high specific surface area, rich structural diversity, and unique energy harvesting property [1–5].

** Full text is published in JAS V. 87, No. 5 (http://springer.com/journal/10812) and in electronic version of ZhPS V. 87, No. 5 (http://www.elibrary.ru/title_about.asp?id=7318; sales@elibrary.ru).

As a 2D carbon nanosheets, graphene oxide (GO) sheets smaller than 10 nm, generally termed graphene quantum dots (GQDs) [6], have excellent properties such as wavelength dependent and photobleaching-resistant fluorescence (FL). Compared with conventional semiconducting quantum dots and fluorescent dyes, GQDs have some fascinating merits such as high specific surface areas, low cytotoxicity, favorable solubility, excellent biocompatibility, and stable FL; these properties make GQDs efficient fluorescent nanomaterials in the field of sensing different analytes from nucleic acids [7, 8], protein kinase [9, 10], biomolecules [11, 12], and metal ions [13, 14].

Manganese oxide (MnO_2) is another kind of newly emerging 2D transition-metal nanomaterials. Single-layer MnO_2 consists of three O−Mn−O atomic layer sandwiches [15]; each Mn coordinates to six O atoms to form an edge-sharing MnO_6 octahedral crystal lattice [16]. Specifically, MnO_2 nanosheets have high specific surface areas and remarkable physisorption to aromatic and conjugated compounds. Furthermore, the *d*–*d* transition of Mn ions in the MnO_6 octahedra of MnO_2 nanosheets results in a broad absorption spectrum (~200−600 nm), which overlaps with the fluorescence emission spectra of the most fluorescent nanomaterials or organic dyes and thus endows MnO_2 nanosheets with intense light absorptive capacity [17]. Moreover, MnO_2 nanosheets themselves have a strong oxidation ability and can oxidize many organic compounds such as ascorbic acid [16], glutathione (GSH) [18–21], etc. Taken together, MnO_2 nanosheets have excellent properties such as low cost and easy preparation, excellent fluorescence quenching ability, oxidation degradative activity, and good biocompatibility, and they have shown increasing potential for application in biosensing and bioimaging [16, 18–21].

Inspired by the above information, we firstly report a facile one-step approach to producing NGQDs−MnO_2 nanosheet sandwich architectures for rapid and selective sensing of glutathione (GSH). The principle of the proposed method is illustrated in Scheme:

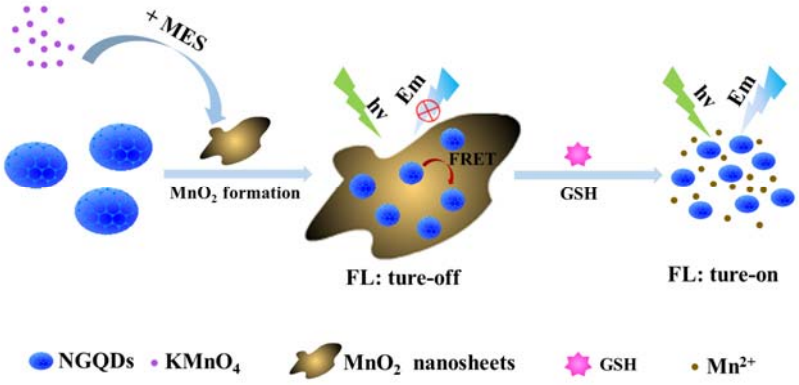

Firstly, a NGQDs–MnO_2 nanocomposite is prepared by the reduction of $KMnO_4$ at room temperature with 2-(N-morpholino)ethanesulfonic acid (MES) in NGQDs aqueous buffer in the presence of active functional groups (e.g., carboxyl and amino groups) on the surface of the NGQDs. NGQDs can easily deposit on the surface of MnO_2 nanosheets by utilizing the strong coordination effect of carboxyl groups with Mn atoms. The fluorescence of NGQDs in this nanocomposite can be significantly quenched due to fluorescence resonance energy transfer (FRET) from NGQDs nanosheet to the deposited MnO_2. Interestingly, the quenched fluorescence can be selectively restored when GSH is introduced, which is the result of the decomposition of the MnO_2 to Mn^{2+} by GSH. On the basis of these findings, highly sensitive and specific sensing of GSH was achieved, and relevant fluorescence on-off-on processes and the sensing mechanism were furthered explored.

Experimental section. $KMnO_4$, GSH (reduced form), H_3PO_4, Na_3PO_4, 4-(2-hydroxyethyl)-1-piperazine-ethane sulfonic acid, glucose (Glu), glycine (Gly), NaCl, ZnCl, KCl, $MgCl_2$, and $CaCl_2$ of analytical grade were purchased from Sinopharm Chemical Reagent Co., Ltd. (China). 2-(N-morpholino)ethane sulfonic acid (MES) was purchased from Shanghai Sangon Biotechnology Co., Ltd. (China). All other reagents of analytical reagent grade were purchased from Sinopharm Chemical Reagent Co., Ltd. (China) and were used without further purification. Ultrapure water obtained from a Millipore water purification system (18.2 MΩ resistivity) was used in all runs.

The FL spectra were recorded with a F-7000 FL spectrophotometer (Hitachi, Japan). Ultraviolet-visible light (UV-vis) absorption spectra were recorded in 1 cm path-length quartz cuvettes on a UV-2450 spectrometer in the range of 250−800 nm. The FL lifetime measurements were performed on a FL-TCSPC spec-

trophotometer (Horiba Jobin Yvon, France).

Preparation of NGQDs. The NGQDs were prepared from graphene sheets (GSs) by a hydrothermal approach as described in the literature [22]. GSs were produced by heating the dried GO to 200°C at a heating rate of 5°C/min and then maintained at 200°C for 2 h in a tube furnace under a nitrogen atmosphere. GSs (0.05 g) were oxidized with concentrated H_2SO_4 and HNO_3 (volume ratio 1:3) for 17 h under mild ultrasonication. The solution was diluted with distilled water (250 mL), and then filtered through a 0.22 mm microporous membrane to remove the acids. The filter cake was collected and redispersed in distilled water (40 mL). The PH was adjusted to 8 with NaOH. The oxidized GS suspension was placed into a poly(tetrafluoroethylene) (Teflon)-lined autoclave and heated at 200°C for 12 h. After cooling to room temperature, the resulting solution was filtered through a 0.22 mm microporous membrane to remove the large tracts of GSs. The brown filtrate was dialyzed in a dialysis bag (retained molecular weight 3500 Da) for 24 h, and the NGQDs prepared by this method show strong blue photoluminescence.

Preparation of NGQDs-MnO_2 sandwich nanocomposite. In a typical reaction, 30 μL different concentrations $KMnO_4$ was added to 970 μL MES buffer (0.1 M, PH 6.0). After that, the resulting mixture was shaken for 8 min until a brown colloid was formed. Then 10 μL NGQDs was mixed with the brown colloid and shaken for 3 min. As a control, MnO_2 nanosheets were prepared in an identical manner but in the absence of NGQDs nanoparticles.

Fluorescence sensing of GSH. For the GSH detection, the sensing solutions were prepared by mixing 10 μL of NGQDs-MnO_2 nanocomposite solutions with 15 μL of different concentrations of GSH in 1.5 mL centrifuge tubes at room temperature. After the incubation of the above mixture solution for about 8 min, the solutions were diluted to 200 μL with ultrapure water and mixed thoroughly. Afterwards, the mixtures were transferred into a 1 cm quartz cuvette, and the fluorescence emission spectra were measured with excitation at 310 nm.

Determining GSH concentration in human whole blood. Human whole blood sample was collected from the Hospital of Nanchang University. The whole blood sample was centrifuged at 12000 rpm for 15 min at room temperature, and the resulting supernatant fluid was diluted 100-fold and added into the FRET-based sensing system immediately. The subsequent operations and fluorescence measurements were the same as above. The concentration of GSH in blood was calculated using the calibration curve obtained in the plasma matrix.

Results and discussion. *Synthesis and characterization of NGQDs and NGQDs−MnO_2 nanosheets sandwich nanocomposite.* NGQDs, which served as fluorescence reporters, were first synthesized by the hydrothermal approach described elsewhere [22]. In brief, GSs were obtained by thermal reduction of GO sheets. The resultant GSs were then subjected to hydrothermal treatment at 200°C, followed by a dialysis process. The FL emission spectra of the obtained NGQDs are shown in Fig. 1a; upon excitation with a 310 nm beam, the FL spectrum of the NGQDs shows a strong peak at ~430 nm. TEM observation clearly confirms the successful production of NGQDs, which are mono-dispersed and spherical in shape with average 1.6 nm diameter (based on statistical analysis of more than 150 dots) (Fig. 1b); the yellow aqueous NGQDs solution emits intense blue luminescence under UV light (365 nm) (inset, Fig 1c). Meanwhile, ultrathin MnO_2 nanosheets were prepared via a one-step approach by reducing $KMnO_4$ in MES buffer. The MnO_2 nanosheets have a broad absorption band from 250 to 600 nm (Fig. 1c) [20, 23]. Obviously, the absorbance spectrum of MnO_2 nanosheets overlaps well with the fluorescence emission of the NGQDs; these results imply that the as-prepared NGQDs and MnO_2 nanosheets should be superior energy donor-acceptor candidates in FRET. Furthermore, the TEM images of the prepared NGQDs-MnO_2 composite clearly show that the NGQDs are well interspersed on the surface of MnO_2 nanosheets (Fig. 1d).

In this work, MES was used to reduce $KMnO_4$ to form amorphous and flake-like MnO_2 nanosheets on the surface of NGQDs. The effect of the $KMnO_4$ concentration on the quenching behaves was studied in a fixed dosage of NGQDs and MES buffer. Figure 2a depicts the FL of NGQDs nanosheets modified with different concentrations of $KMnO_4$. As expected, the FL intensity of NGQDs nanosheets decreased as the $KMnO_4$ concentration increased and trended to a minimum value at 80 mM $KMnO_4$. Furthermore, it can also be clearly observed that the color of NGQDs-MnO_2 nanocomposite became deeper with increase in $KMnO_4$ concentration (Fig. 2b). Thus, in view of reducing unspecific interference in the process of experimental, a medium concentration 14 mM $KMnO_4$ was used in the following experimental procedures.

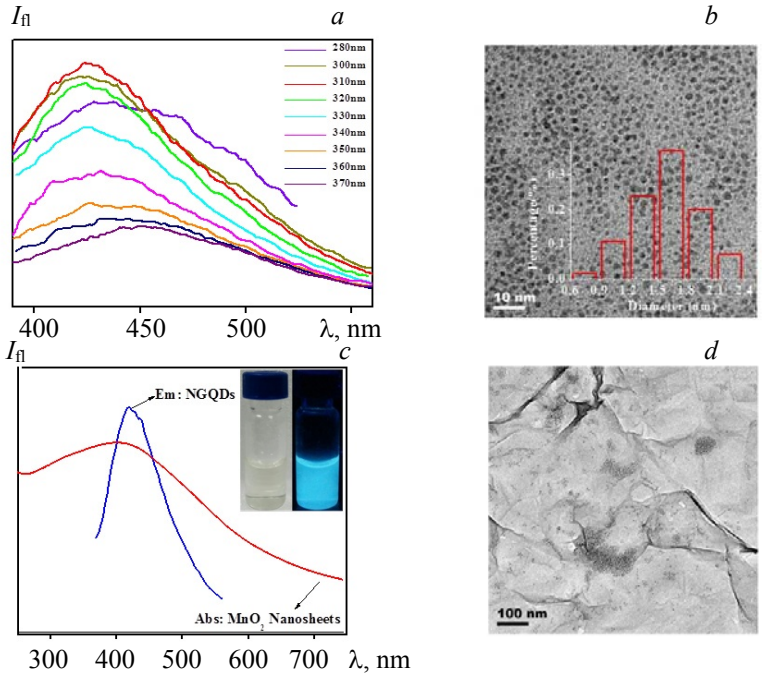

Fig. 1. a) Fluorescent spectra of the NGQDs at different excitation wavelengths. b) TEM image of the as-prepared NGQDs. c) Spectral overlap showing the UV-vis absorption spectrum of MnO_2 nanosheets (red) and the fluorescence emission spectrum of the NGQDs (blue). Inset: photographs of the above NGQDs solution excited by daylight (left) and a 365 nm UV lamp (right). d) TEM image of the NGQDs–MnO_2 nanosheets composite.

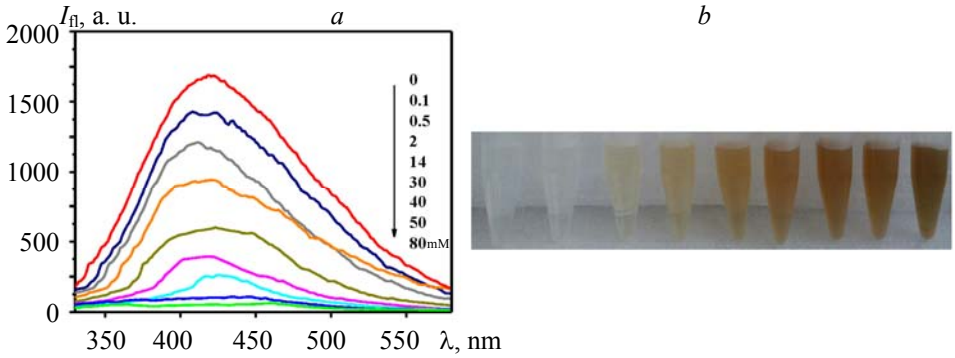

Fig. 2. a) Fluorescence spectra of NGQDs nanosheets prepared by different concentrations of $KMnO_4$; excitation wavelength 310 nm. b) Corresponding photographs of the MnO_2-modified NGQDs assembly aqueous solution formed at a series of different $KMnO_4$ concentrations.

Fluorescence sensing of GSH based on the NGQDs-MnO_2 nanocomposite. To demonstrate the applicability of the developed FL sensor for quantitative detection of GSH, we investigated the FL response of NGQDs-MnO_2 nanocomposite after incubation with GSH at different concentrations for ~7 min in aqueous solutions. The FL of NGQDs nanosheets was shown to gradually restore with increasing concentration of GSH. Namely, the restored FL was dependent on the introduced amount of GSH (Fig. 3A). When the concentration of GSH was increased to 400 μM, no further increase in FL can be observed, showing that the sensing response had reached the maximum. The inset in Fig. 3A shows a plot of the FL intensity ratio $(F - F_0)/F_0$ (F_0 and F are the FL intensity of NGQDs-MnO_2 nanocomposite at ~430 nm in the absence and presence of GSH, respectively) enhancement against the concentration of GSH. The fitted curve can be used for the quantification of GSH with a correlation coefficient of 0.992. The FL ratio has a linear correlation

with the concentration of GSH over a broad range from 0 to 400 μM (inset, Fig. 3A). The detection limit (sensitivity threshold) was calculated to be 27 pM by evaluating the average response of the blank plus three times standard deviation ($S/N = 3$).

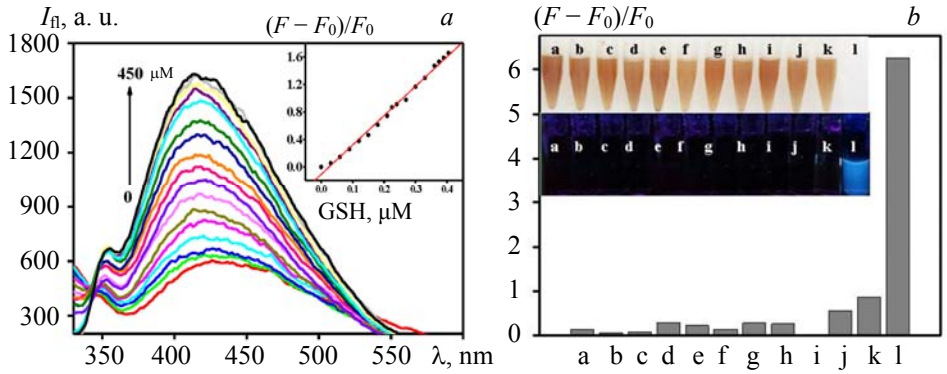

Fig. 3. a) Fluorescence spectra of NGQDs nanosheets prepared by different concentrations of GSH (0–450 μM). b) FL spectra of NGQDs-MnO_2 nanocomposite in the presence of different concentrations of GSH (0−450 μM). The inset shows the plot of the fluorescence intensity ratio versus GSH concentration (0, 30, 60, 90, 120, 150, 180, 210, 225, 240, 270, 300, 330, 360, 370, 390, 400, 450 μM). The fluorescence emission intensity at ~430 nm was measured with an excitation wavelength of 310 nm. (B) Selectivity of the NGQDs-MnO_2 nanocomposite GSH sensing platform over glucose (a), glutamic acid (b), glycine (c), Ca^{2+} (d), Zn^{2+} (e), Na^+ (f), K^+ (g), Mg^{2+} (h), Mn^{2+} (i), homocysteine (j), cysteine (k), and GSH (l). (F_0: FL intensity of the sensor; F: FL intensity of the sensor in the presence of interferents)

To assess the selectivity of NGQDs-MnO_2 nanocomposite for GSH, the influence of some common species, especially in the human body, including glucose, metal ions (Ca^{2+}, Zn^{2+}, Na^+, K^+, Mg^{2+}, and Mn^{2+}) and amino acids (glutamic acid, glycine, homocysteine, and cysteine), was widely investigated in aqueous solutions. The experimental results are illustrated in Fig. 3B. The NGQDs-MnO_2 nanocomposite exhibited a remarkable increase in FL toward GSH (100 μM). In marked contrast, no obvious FL intensity changes could be observed with other molecules (Fig. 3B). Among them, the GSH analog cysteine (Cys) and homocysteine (HCys) can also cause some FL recovery to this nanocomposite. Nevertheless, the concentrations of these interferents in human whole blood is generally much lower than that of GSH [20, 24–26]. Thus, the NGQDs-MnO_2 nanocomposite can be implemented as a selective platform for sensing of the GSH from other interfering molecules.

Process monitoring and sensing mechanism. The large lateral dimensions and high surface areas of layered MnO_2 enables easy absorption of fluorescent nanomaterials, which leads to efficient FL quenching [16, 18–21, 27–29]. In light of the well-defined energy harvesting property of MnO_2, we supposed that a FRET process from the excited NGQDs to the quencher MnO_2 would have occurred. To prove this, time-resolved FL spectra of the NGQDs and the NGQDs-MnO_2 nanocomposite were measured. Due to differences in the distribution of complex luminescent pathways resulting from multiple GQD species, the FL intensity of NGQDs following multi-exponential models containing two lifetimes are acquired (Fig. 4a). It is found that the FL lifetime of the NGQDs does not change in any obvious manner with the addition of MnO_2 nanosheets. A possible explanation for the fluorescence decay of NGQD-MnO_2 being lower than NGQD is the FRET process. As indicated in Fig. 1c, the absorption spectrum of MnO_2 nanosheets overlaps well with the fluorescence emission of NGQD. Consequently, in the presence of MnO_2 nanosheets, the FRET from the NGQD to the nonfluorescent MnO_2 nanosheets is enhanced [26, 30–32]. The unchanged FL lifetime and the linear Stern–Volmer plot (inset of Fig. 3a) imply that the quenching of NGQDs by MnO_2 nanosheets obeys a simple static quenching mechanism. That is, under the influence of the strong coordination effect between carboxyl groups on the surface of the NGQDs with Mn atoms, NGQDs can easily deposit on the surface of MnO_2 nanosheets, whereas MnO_2 nanosheets have a broad absorption band that overlaps significantly with the blue emission of NGQDs (Fig. 1c); thus the as-prepared NGQDs should be a superior energy donor, and the MnO_2 nanosheets are the energy harvesting unit of the process in FRET, which subsequently leads to the FL quenching of the NGQDs upon the action of the static quenching.

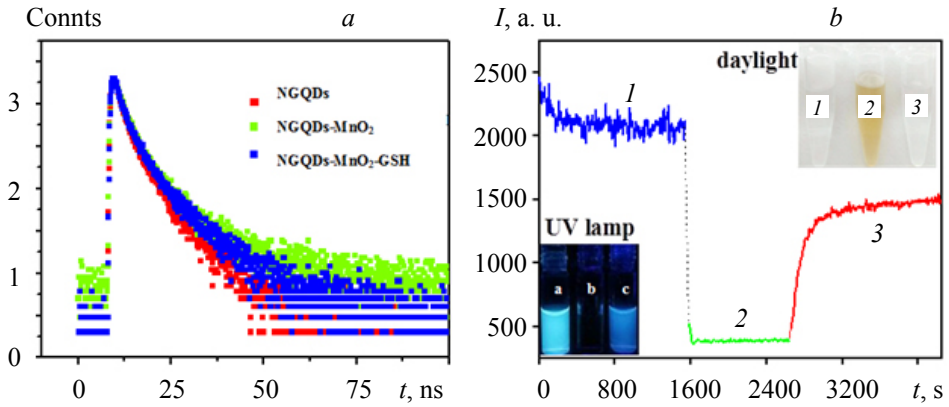

Fig. 4. a) FL decays of the NGQDs, NGQDs-MnO_2 nanosheets composite, and NGQDs-MnO_2-GSH systems (10 μL NGQDs, 30 μL 40 mM $KMnO_4$, 970 μL 0.1 mM MES, and 360 μM GSH). b) FL response of NGQDs (1) in the presence of MnO_2 nanocomposite (2), and in the presence of MnO_2 nanocomposite/GSH (360 μM) (3) as a function of time.

Then the addition of GSH to NGQDs-MnO_2 nanocomposite leads to the FL recovery of the NGQDs. This would be the result of GSH–mediated reduction and decomposition of MnO_2 nanosheets, which are accompanied by luminescence recovery of the NGQDs. The reaction of MnO_2 to Mn^{2+} in the presence of GSH can be represented as the follows [20, 26, 28, 33]:

$$MnO_2 + 2GSH + 2H^+ \rightarrow Mn^{2+} + GSSG + 2H_2O$$

To further test the effect of the NGQDs FL quenching by the MnO_2 nanosheets and the restoration of the NGQDs-MnO_2 nanocomposite by the GSH, the kinetic behavior of the above- mentioned interaction was further studied by monitoring the FL changes as a function of time. As shown in Fig. 4b, the FL of the alone NGQDs is stable for the period of 0–1600 s and shows no obvious variations on the 310 nm excitation wavelength (curves 1). After addition of $KMnO_4$ and MES, the FL of the NGQDs is immediately quenched due to the formation of the MnO_2 nanosheets and the occurrence of the FRET (curves 2). Then, the FL of the NGQDs is gradually restored to a degree of 75% by mixing with GSH in the NGQDs-MnO_2 systems for about ~480 s (curves 3). The insets correspond to process 1, 2, and 3 under daylight and UV lamp.

Selectivity of NGQDs-MnO_2 nanocomposite-based sensoring system. To further test the specificity of this nanosystem toward GSH, other possible interfering species including various buffers, metal ions, and amino acids were mixed with the solution of MnO_2-modified NGQDs. As shown in Fig. 5, the NGQDs-MnO_2 nanocomposite exhibited a remarkable FL increase toward GSH at the concentration 200 μM. In marked contrast, no obvious FL intensity changes could be observed with other interferents. Among them, Cysteine (Cys) and homocysteine (HCys) can also cause some FL response to the proposed nanocomposite. Nevertheless, the content of Cys or HCys (μM levels) in human whole blood is much lower than that of GSH (mM levels) [20, 34]. Thus, the NGQDs-MnO_2 nanocomposite can be implemented as a highly selective platform for sensing GSH in human whole blood samples without significant interference.

Blood GSH may serve as an accurate indicator of GSH status in human subjects, which usually has been considered as an essential role in some diseases and their therapy [35]. Thus, the practicability of the proposed sensing platform for GSH in human whole blood samples (donated by the local Hospital) is examined after pretreating the whole blood using a routine procedure (details in the Supporting Information). The 100-fold diluted human blood samples were directly added into the sensing system, the corresponding FL intensities were recorded, and the recoveries of the proposed method were calculated. The results are shown in Table 1.

TABLE 1. Determination results of GSH in diluted human blood sample

Sample No.	Measured, μM	Added, μM	Found, μM	RSD (n=3)	Recovery, %
1	7.5	100	102.5	3.6	95
2	8.4	200	201.3	4.3	97
3	8.7	300	327.4	5.8	106

The obtained GSH concentration ranges in human blood were in agreement with reports in the literature [36, 37]. Recoveries of different known amounts of added GSH were obtained from 95 to 106%. The good recovery showed that the developed NGQDs-MnO_2 nanocomposite based method possessed the feasibility and reliability for real clinical sample analysis.

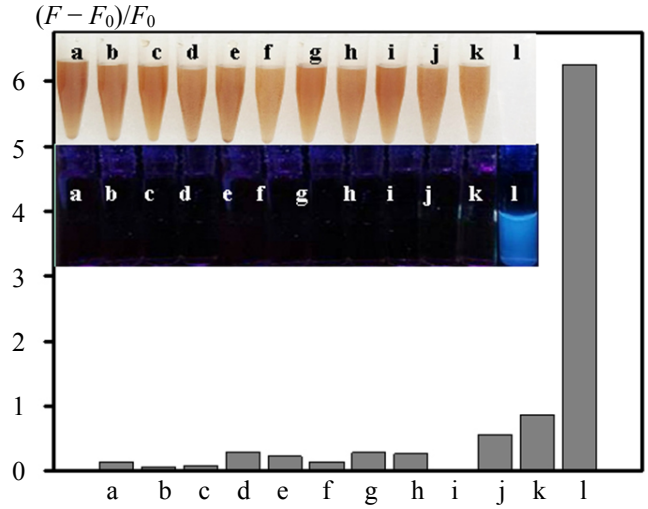

Fig. 5. FL responses $(F - F_0)/F_0$ of the NGQDs-MnO_2 nanocomposite sensing platform towards GSH and interferents: a) PBS; b) HEPES; c) glutamic acid; d) glycine; e) Zn^{2+}; f) Na^{+}; g) K^{+}; h) Mg^{2+}; i) Mn^{2+}; j) Cys; k) Hcys; l) GSH (F_0: FL intensity of the sensor; F: intensity of the sensor in the presence of GSH and interferents. The concentration of GSH, Cys, and Hcy is 200 μM; the concentration of other interferents is 10 mM.

Conclusions. A novel FRET-based GSH sensing platform using fluorescent NGQDs and MnO_2 nanosheets as energy donor-acceptor pairs has been designed and fabricated for the first time. The proposed strategy displays multifaceted advantages: 1) it is a very simple and straightforward technique to detect GSH without any troublesome procedures and large-scale expensive instrument; 2) the construction of the nitrite ion sensor is very facile and low-cost without any requirement for chemical labeling and modification of probes; 3) the detection time was very fast and the whole process required only about 7 min, which is essential for construction assays for biological systems. Finally, relevant investigations on fluorescence on-off-on processes and sensing mechanisms have been proposed, which can be used for further biological and clinical diagnostics applications.

Acknowledgments. This work is supported by the National Natural Science Foundation of China (21605075; 21365015; 31660491; 31960207) and Natural Science Foundation of Jiang Xi Province 20181BAB203020, and Interdisciplinary Innovation Fund of Nanchang University (IIFNCU, 9166-27060003-YB17).

Compliance with ethical standards. This study was performed in accordance with the ethical standards of the 1964 Helsinki Declaration on Biomedical Research Involving Human Subjects and its later amendments.

REFERENCES

1. M. Xu, T. Liang, M. Shi, H. Chen, *Chem. Rev.*, **113**, 3766–3798 (2013).
2. X. Huang, Z. Zeng, H. Zhang, *ChSRv*, **42**, 1934–1946 (2013).
3. M. Chhowalla, H. S. Shin, G. Eda, L.-J. Li, K. P. Loh, H. Zhang, *Nature Chem.*, **5**, 263–275 (2013).
4. C. N. R. Rao, A. K. Sood, K. S. Subrahmanyam, A. Govindaraj, *Angew. Chem. Int. Ed.*, **48**, 7752–7777 (2009).
5. M. J. Allen, V. C. Tung, R. B. Kaner, *Chem. Rev.*, **110**, 132–145 (2009).
6. L. Ponomarenko, F. Schedin, M. Katsnelson, R. Yang, E. Hill, K. Novoselov, A. Geim, *Science,* **320**, N 5874, 356–358 (2008).
7. P. Zhang, Y. Zhuo, Y. Chang, R. Yuan, Y. Chai, *Anal. Chem.*, **87**, 10385–10391 (2015).

8. Z. S. Qian, X. Y. Shan, L. J. Chai, J. J. Ma, J. R. Chen, H. Feng, *Nanoscale*, **6**, 5671–5674 (2014).
9. Y. Wang, L. Zhang, R. P. Liang, J. M. Bai, J. D. Qiu, *Anal. Chem*., **85**, 9148–9155 (2013).
10. H. F. Zhao, R. P. Liang, J. W. Wang, J. D. Qiu, *Chem. Commun*., **51**, 12669–12672 (2015).
11. H. Dong, W. Gao, F. Yan, H. Ji, H. Ju, *Anal. Chem*., **82**, 5511–5517 (2010).
12. X. Ran, H. Sun, F. Pu, J. Ren, X. Qu, *Chem. Commun*., **49**, 1079–1081 (2013).
13. S. Li, Y. Li, J. Cao, J. Zhu, L. Fan, X. Li, *Anal. Chem*., **86**, 10201–10207 (2014).
14. Y. Liu, D. Y. Kim, *Chem. Commun*., **51**, 4176–4179 (2015).
15. B. A. Pinaud, Z. Chen, D. N. Abram, T. F. Jaramillo, *J. Phys. Chem. C*, **115**, 11830–11838 (2011).
16. W. Zhai, C. Wang, P. Yu, Y. Wang, L. Mao, *Anal. Chem*., **86**, 12206–12213 (2014).
17. D. He, X. He, K. Wang, X. Yang, X. Yang, X. Li, Z. Zou, *Chem. Commun*., **50**, 11049–11052 (2014).
18. J. Yuan, Y. Cen, X. J. Kong, S. Wu, C. L. Liu, R. Q. Yu, X. Chu, *ACS Appl. Mater. Interfaces*, **7**, 10548–10555 (2015).
19. Y. Wang, K. Jiang, J. Zhu, L. Zhang, H. Lin, *Chem. Commun.*, **51**, 12748–12751 (2015).
20. X. L. Zhang, C. Zheng, S. S. Guo, J. Li, H. H. Yang, G. Chen, *Anal. Chem*., **86**, 3426–3434 (2014).
21. H. M. Meng, Z. Jin, Y. Lv, C. Yang, X. B. Zhang, W. Tan, R. Q. Yu, *Anal. Chem*., **86**, 12321–12326 (2014).
22. D. Pan, J. Zhang, Z. Li, M. Wu, *Adv. Mater*., **22**, 734–738 (2010).
23. G. Zhao, J. Li, L. Jiang, H. Dong, X. Wang, W. Hu, *Chem. Sci*., **3**, 433–437 (2012).
24. F. Yu, P. Li, B. Wang, K. Han, *J. Am. Chem. Soc.*, **135**, 7674–7680 (2013).
25. L. El-Khairy, P. M. Ueland, H. Refsum, I. M. Graham, S. E. Vollset, *Circulation*, **103**, 2544–2549 (2001).
26. Y. Wang, K. Jiang, J. Zhu, L. Zhang, H. Lin, *Chem. Commun.*, **51**, 12748–12751 (2015).
27. Y. Yuan, S. Wu, F. Shu, Z. Liu, *Chem. Commun*., **50**, 1095–1097 (2014).
28. R. Deng, X. Xie, M. Vendrell, Y. T. Chang, X. Liu, *J. Am. Chem. Soc*., **133**, 20168–20171 (2011).
29. N. Li, W. Diao, Y. Han, W. Pan, T. Zhang, B. Tang, *Chemistry–a Eur. J.*, **20**, 16488–16491 (2014).
30. X. Wang, D. Wang, Y. Guo, C. Yang, X. Liu, A. Iqbal, W. Liu, W. Qin, D. Yan, H. Guo, *Biosens. Bioelectron*., **77**, 299–305 (2016).
31. Y. Mi, X. Lei, H. Han, J. Liang, L. Liu, *Anal. Methods*, **10**, 4170–4177 (2018).
32. X. Yan, Y. Song, C. Zhu, J. Song, D. Du, X. Su, Y. Lin, *ACS Appl. Mater. Interfaces*, **8**, 21990–21996 (2016).
33. Z. Z. Dong, L. Lu, C. N. Ko, C. Yang, S. Li, M. Y. Lee, C. H. Leung, D. L. Ma, *Nanoscale*, **9**, 4677–4682 (2017).
34. D. Feng, Y. C. Song, W. Shi, X. H. Li, H. M. Ma, *Anal. Chem*., **85**, 6530–6535 (2013).
35. D. Tian, Z. Qian, Y. Xia, C. Zhu, *Langmuir*, **28**, 3945–3951 (2013).
36. F. Michelet, R. Gueguen, P. Leroy, M. Wellman, A. Nicolas, G. Siest, *Clin. Chem.*, **41**, 1509–1517 (1995).
37. R. Deicher, F. Ziai, C. Bieglmayer, M. Schillinger, W. H. Horl, *J. Am. Soc. Nephrol.*, **16**, 1811–1818 (2005).